

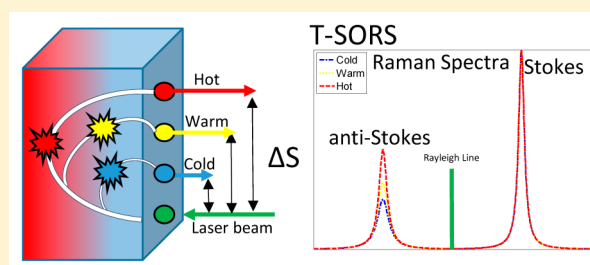
# Temperature Spatially Offset Raman Spectroscopy (T-SORS): Subsurface Chemically Specific Measurement of Temperature in Turbid Media Using Anti-Stokes Spatially Offset Raman Spectroscopy

Benjamin Gardner,<sup>†</sup> Pavel Matousek,<sup>\*,‡</sup> and Nicholas Stone<sup>\*,†</sup>

<sup>†</sup>Biomedical Physics, School of Physics, College of Engineering, Mathematics and Physical Sciences, University of Exeter, Exeter, Devon EX4 4QL, United Kingdom

<sup>‡</sup>Central Laser Facility, Research Complex at Harwell, STFC Rutherford Appleton Laboratory, Harwell, Oxfordshire OX11 0QX, United Kingdom

**ABSTRACT:** Here we propose and demonstrate a new analytical method for the noninvasive measurement of subsurface temperatures within diffusely scattering (turbid) media in combination with high chemical selectivity. The method is based upon the first combination of Stokes/anti-Stokes light scattering measurements and the recently developed spatially offset Raman spectroscopy (SORS). This approach has been conceptually demonstrated by measuring material-specific temperatures within a turbid sublayer of poly(tetrafluoroethylene) (PTFE) through a highly diffusely scattering overlayer of poly(oxymethylene) POM (3 mm thick). Root-mean-square errors (RMSEs) of 0.16–0.71 °C were achieved when measuring temperatures over ranges between 24 and 45 °C. This unique capability complements the array of existing, predominantly surface-based, temperature measurement techniques. It paves the way for a wide range of topical applications including subsurface, chemically specific, noninvasive temperature measurements within translucent media including the human body, subsurface monitoring of chemical or catalytic processes in manufacture quality and process control, and research.



The measurement of subsurface temperature in turbid media is a highly topical area in analytical sciences with potential applications ranging from monitoring subsurface temperature in the human body to monitoring chemical and materials processes during production and storage. Current mainstream methods, such as contact thermometers and infrared probes, are confined to measuring only the surface temperature in non-IR transparent or diffusely scattering media. Moreover, for accurate temperature measurements using thermography, the emissivity of the object needs to be known and correctly calibrated for. This value can theoretically range from 1 if the object acts as a perfect blackbody to 0 (completely nonemitting).<sup>1</sup> The precision of these different techniques can vary, with the resolvable temperature for thermocouples at 0.0025 °C, whereas the precision of infrared thermography has an average of ~0.02–0.1 °C.<sup>1,2</sup>

There are a couple of techniques capable of measuring temperature at depth in turbid media. Microwave-based temperature sensing can penetrate deep inside turbid media, although these sensors have limited spatial resolution due to the long wavelength of radiation used and do not provide high selectivity to chemical subcomponents.<sup>3</sup> Another approach to deep temperature measurement is magnetic resonance imaging (MRI) thermometry.<sup>4</sup> However, as this is reliant upon temperature-dependent water proton resonance frequency shifts, this mechanism is not applicable to all materials that might be monitored. There are other temperature-dependent properties that can be probed with MRI, such as  $T_1$  (spin–

lattice) relaxation time and  $T_2$  (spin–spin) relaxation time of water molecules. Both of these approaches are complex to accurately calibrate and are limited to specific tissue types.<sup>4</sup> In addition, MRI methods are often prohibitively costly for many practical applications.

Conventional Raman spectroscopy presents a niche technique for temperature measurements with high chemical specificity but is confined to near surfaces within diffusely scattering samples. The principle relies on the measurement of both the Stokes and anti-Stokes components of the Raman spectrum (Figure 1a), and the temperature is derived from the ratio of intensities of counterpart Stokes and anti-Stokes lines.<sup>5,6</sup> The ratio is temperature-dependent due to the fact that anti-Stokes Raman bands are solely due to vibrationally excited molecules, whereas the Stokes lines derive their intensity from molecules both in the ground as well as vibrationally excited states. The intensity ratio can be approximated for normal Raman and neglecting wavelength dependence of Raman scattering by the following formula:

$$\frac{I_{\text{anti-Stokes}}}{I_{\text{Stokes}}} = \exp(-E/kT) \quad (1)$$

Received: September 3, 2015

Accepted: December 1, 2015

Published: December 1, 2015

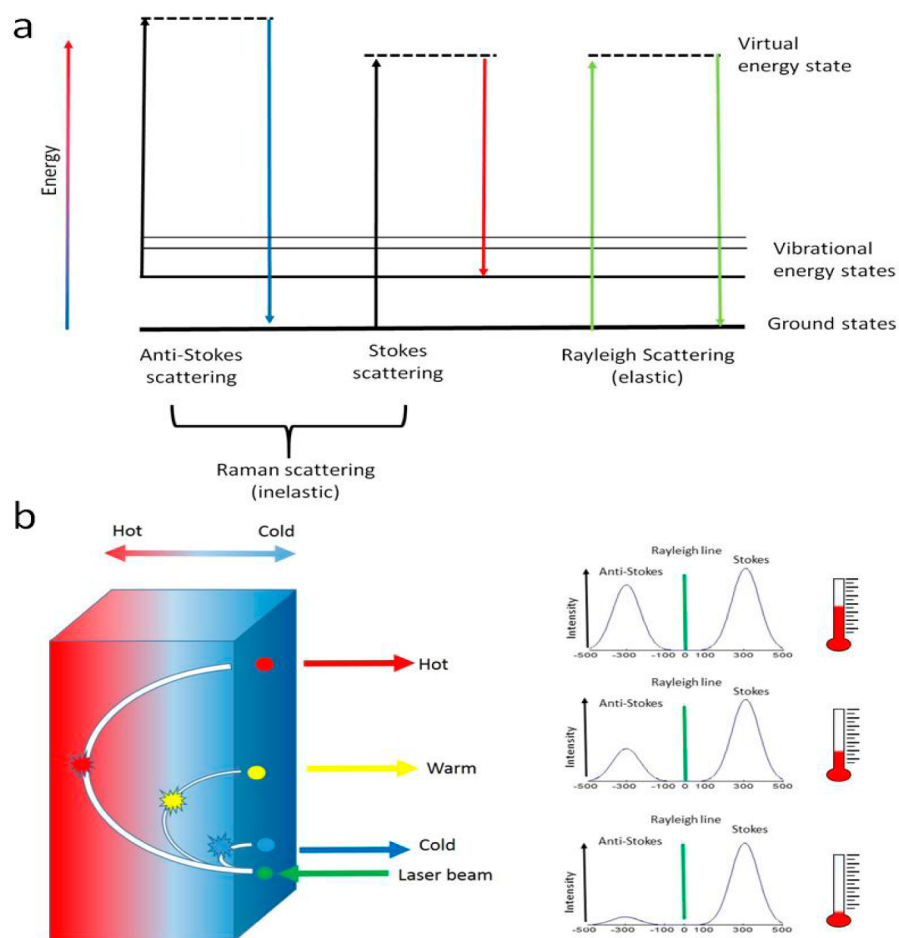


**Figure 1.** Schematic diagram of T-SORS thermometry concept. (a) Energy diagram for Stokes and anti-Stokes Raman scattering. Most photons scatter with the same energy, elastic scattering. At room temperature most molecules will be in the ground vibrational energy state, so Stokes scattering is the dominant Raman process where the molecule is promoted to a higher vibrational energy level. However, some molecules will be in an excited state and fall to the ground state and transfer some energy to the photon. (b) Concept schematic of T-SORS. In this example, with a cold surface and warm interior, as the spatial offset between the illumination point and collection point increases there is a relative increase in the anti-Stokes contribution in the spectra originating from the warmer sublayer.

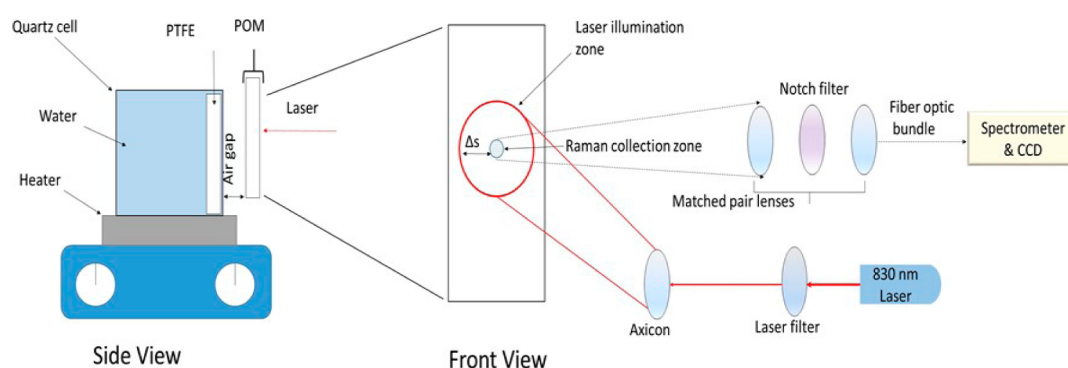


**Figure 2.** Schematic of the inverse SORS setup. The 830 nm laser beam is passed through an axicon, creating a ring-shaped beam. This size of the ring is controlled by how close the axicon is to the sample. The backscattered Raman photons are collected by a 50 mm diameter  $f = 60$  mm lens, filtered by a Kaiser notch filter (830 nm), focused with a 50 mm diameter  $f = 60$  mm lens onto a fiber bundle (Ceramoptic). The circular cross section bundle is converted into a line of fibers for entry into a Kaiser HoloSpec 1.8i spectrometer with a low-dispersion transmission grating and an Andor iDus 420 deep depletion CCD.

where  $k$  is the Boltzmann's constant ( $1.3807 \times 10^{-23} \text{ J K}^{-1}$ ),  $T$  is the temperature (K), and  $E$  is the first vibrational state energy (J).

A new prospect for deep subsurface probing of chemical composition in turbid materials using Raman spectroscopy recently emerged from the advent of spatially offset Raman

spectroscopy (SORS).<sup>7,8</sup> SORS enables the noninvasive chemical analysis of stratified turbid media and the subsequent recovery of pure Raman signatures of individual layers by numerical processing. SORS has opened the way for a host of new applications including the scanning of liquids in sealed

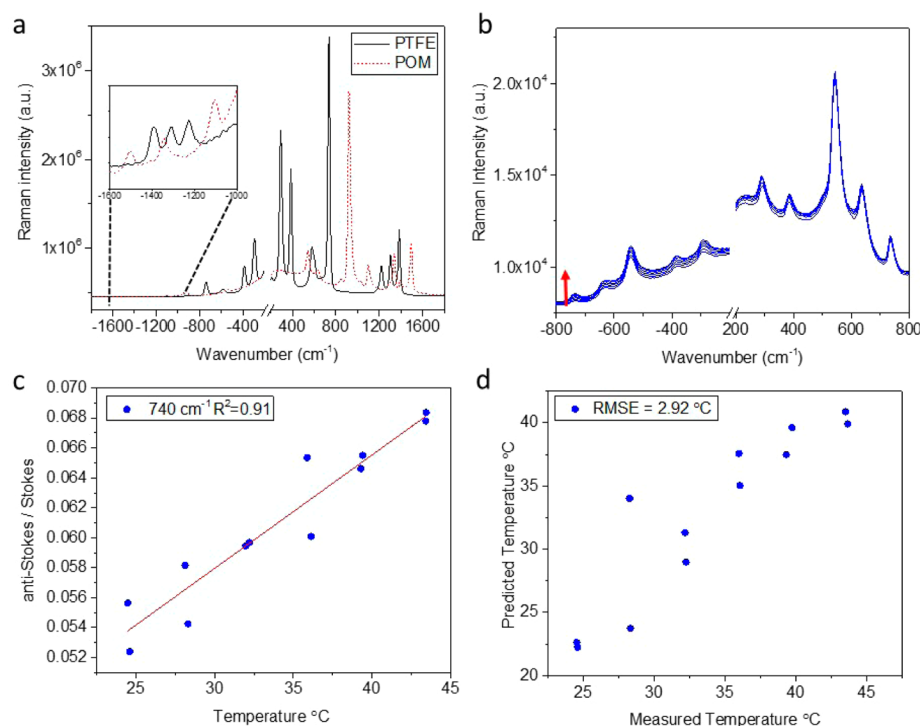


**Figure 3.** Anti-Stokes–Stokes Raman spectra of plastics. (a) The anti-Stokes–Stokes Raman spectra of the two plastic layers, poly(tetrafluoroethylene) (PTFE) and poly(oxymethylene) (POM). (b) Raman spectra of PTFE measured behind POM at seven temperatures (\*PTFE univariate temperature calibration peak at  $\sim 740\text{ cm}^{-1}$ ). (c) Calibration curve for the selected PTFE peak. (d) Correlation between the predicted and observed temperature for control measurements.

bottles in aviation security, the monitoring of final products and incoming raw materials in pharmaceutical quality control, and also paves the way for noninvasive breast cancer and bone disease diagnosis.<sup>9,10</sup>

Here we propose a significant new capability by combining Stokes/anti-Stokes scattering measurements with SORS to demonstrate T-SORS, or temperature-SORS, for the first time. The use of this proposed combination of SORS and anti-Stokes to Stokes line measurements enables the accurate probing of temperatures in specific materials buried deeply within diffusely scattering samples (Figure 1b). T-SORS provides a unique and exceptional chemical selectivity to individual, chemically distinct, sample subcomponents combined with conceptual simplicity unavailable from alternative subsurface sensing methods.

## EXPERIMENTAL METHODS

The instrument used for these experiments consisted of a home-built spatially offset Raman system. It relies upon the concept that when Raman spectra of diffusely scattering media are collected at a location that is separated by a distance  $\Delta s$  from the laser illumination, the signal generated contains contributions from the materials buried beneath the surface of the material being probed. The larger the value of  $\Delta s$  the larger the relative contribution of the signals from the buried regions of the sample. In this system an axicon lens was used to produce a ring-shaped laser illumination zone, and the Raman spectra were collected from the center of the ring. This form of SORS is termed inverse SORS.<sup>11</sup>

Figure 2 presents a schematic diagram of the experimental setup for temperature measurements with T-SORS. The excitation wavelength was 830 nm and was delivered by a spectrum-stabilized laser (Innovative Photonic Solutions: I0830MM0350MF-EM) passed through three 830 nm band-

pass filters (Semrock) to clean up the spectrum. Raman spectra were collected on a deep depletion CCD camera (Andor iDus-420) coupled to a Kaiser spectrometer (Holospec 1.8i). All Raman spectra were collected for a total of 60 s ( $12 \times 5$  s acquisitions).

The sample consisted of two turbid layers: the top layer was poly(oxymethylene) (POM) held at near ambient temperature  $\sim 22\text{ }^{\circ}\text{C}$ , and the sublayer was poly(tetrafluoroethylene) (PTFE) maintained at various temperatures. Both the layers were 3 mm thick. The PTFE was kept in a thermostatically controlled water bath within a large quartz cell. For the purposes of this experiment a temperature insulating air gap of  $\sim 5$  mm was present between the POM and quartz cell, to minimize heat transfer from the underlying sample (PTFE).

For the experiments carried out between 24 and  $45\text{ }^{\circ}\text{C}$ , four repeat experiments each containing five spectra were performed, at the six temperature points. The PTFE temperature was varied between 24 and  $45\text{ }^{\circ}\text{C}$  in  $\sim 3.5\text{ }^{\circ}\text{C}$  increments; the temperature was allowed to stabilize for a minimum of 30 min between measurements. The experiment was also carried out over a smaller temperature range of  $\sim 2\text{ }^{\circ}\text{C}$ , where the temperature was incrementally increased by  $\sim 0.5\text{ }^{\circ}\text{C}$  between temperature points. Spectra were acquired under the same experimental conditions as described above.

Temperature was measured from the PTFE in the quartz cell by two type K thermocouples connected to a Pico-TC-08 thermocouple data logger. The temperature was measured every second during measurements, and the average temperature over the two thermocouples was used.

The POM layer was moved in and out of its position using a Standa (8MTF) motorized  $xy$ -stage. This also allowed the independent measurement of the PTFE Raman spectra without the POM layer for each experiment.

The data was analyzed using Matlab 2014, both by fitting a Gaussian curve to the chosen PTFE band at  $740\text{ cm}^{-1}$  and then using the partial least-squares regression (PLS) approach. The PLS models were created from the first half of the data and validated with the second half (test set).

## RESULTS AND DISCUSSION

The Raman spectra of the two diffusely scattering materials PTFE and POM when measured independently (at room temperature) are shown in Figure 3a. Both materials have Raman bands in the range of  $200\text{--}1500\text{ cm}^{-1}$ , and these were all detectable in the anti-Stokes region of the spectrum on the inverse SORS system, albeit at a diminished intensity (relative to the Stokes region) as expected at room temperature. As seen in the spectra, both materials have Raman bands that overlap, in addition to nonoverlapping bands. Initially, to simplify analysis, nonoverlapping Raman bands of the sublayer PTFE were chosen (Figure 3b) for determining the anti-Stokes/Stokes intensity ratio.

Due to instrument effects, such as the efficiency of the CCD camera and diffraction grating as a function of wavelength, as well as absorption of Raman photons, the theoretically predicted anti-Stokes/Stokes ratio and experimentally determined values will not necessarily match. However, this is not important as temperature was predicted based on the fit of the ratio from experimentally determined data, or using a PLS model.

By use of the calculated calibration curves obtained (Figure 3c), it was possible to predict the temperature in the test set of measurements for the sublayer PTFE from the relative intensities of the chosen Raman band to  $2.92\text{ }^{\circ}\text{C}$  root-mean-squared error, RMSE (Figure 3d).

When it is viable to equilibrate the buried material, i.e., PTFE, to the same temperature as the external covering material, in this case POM, it is then possible to use a model of PTFE heating alone and calibrate the subsurface measurements to this model without need to read subsurface temperature. Figure 4 shows the

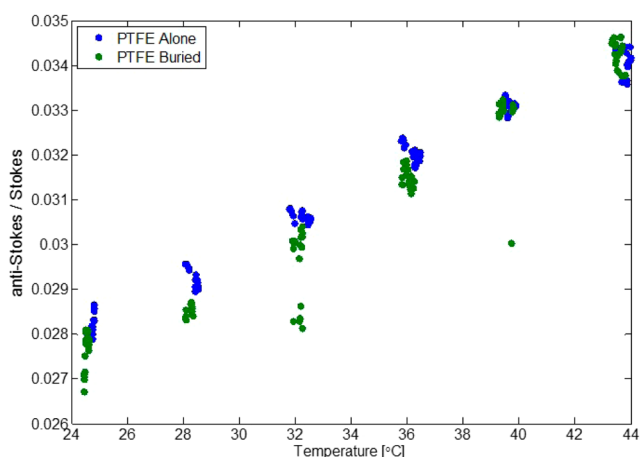


**Figure 4.** Anti-Stokes to Stokes Raman intensity ratios of spectra of PTFE (blue) and PTFE-buried (green) after equilibrium calibration.

anti-Stokes/Stokes of PTFE heating versus the anti-Stokes/Stokes of PTFE being heated when behind POM. From using data when there is a thermal equilibrium between both materials, i.e., at room temperature, it was possible to calibrate non-invasively the anti-Stokes/Stokes of when PTFE is buried and predict the temperature to an RMSE of  $\sim 2.4\text{ }^{\circ}\text{C}$  using the PTFE model of heating.

Clearly, using a univariate approach is in effect throwing away potentially relevant data. To evaluate whether making use of the whole spectrum for temperature prediction was able to improve the precision of the method, we employed the multivariate method of PLS. PLS is a commonly used method in chemometrics for both regression (PLS-R) and discriminant analysis (PLS-DA). It is a multivariate technique and so takes into account all variables simultaneously. The PLS algorithm extracts a number of latent variables from the training data matrix such that they contain the maximum variation that is covariate with a response variable (e.g., concentration for regression) or in this case temperature.

In constructing a PLS model it is crucial to select the optimal number of components; too few and the model could be underfit, while too many can lead to overfitting, either of which can lead to a poor predictive ability with future samples. Here a leave-every-other-replicate-out PLS model was constructed from the replicate sets of experimental data; the number of PLS components versus the percentage of explained variance (Figure 5a) shows that most of the variance is explained within the first five components. As is shown (Figure 5b), the constructed model shows a close fit with an  $R^2$  value of 0.99, better than that achieved for the band used in the univariate models constructed using Gaussian fitting of peaks (Figure 3c). Furthermore, the prediction accuracy is improved; when tested on the test set of data, a lower RMSE is achieved ( $0.71\text{ }^{\circ}\text{C}$ ) using PLS (Figure 5c).

To further validate and evaluate the potential ability of T-SORS to measure temperature of subsurface samples with clinical relevance, a much smaller temperature range was investigated. In this experiment, the temperature of PTFE was incrementally increased in  $\sim 0.5\text{ }^{\circ}\text{C}$  steps over a range of  $36.5\text{--}38.5\text{ }^{\circ}\text{C}$ . A new PLS model was developed over the temperature range; again most of the variance ( $>98\%$ ) was explained in the first five PLS components (Figure 6a). A good fit was seen in the calibration set of data  $R^2 = 0.99$  (Figure 6b), and an RMSE of  $0.16\text{ }^{\circ}\text{C}$  was achieved in the prediction set of data (Figure 6c).

The improvement of the RMSE of prediction from  $0.71$  to  $0.16\text{ }^{\circ}\text{C}$  is attributed to the much smaller  $\sim 0.5\text{ }^{\circ}\text{C}$  temperature increments used. This result is of particular medical relevance as it encompasses clinically relevant values of subsurface temperatures. It should be noted that further optimization of the concept is envisaged by improving data preprocessing and experimental apparatus to include biological material. The results presented here represent only the first conceptual demonstration.

## CONCLUSIONS

Here we have made the first demonstration of T-SORS, where the temperature of a subsurface material can be measured with chemical specificity and through another diffusely scattering material. Use of a multivariate approach, PLS, allowed a more accurate predictor of the subsurface material temperature, compared to utilization of Stokes/anti-Stokes ratios of selected peak intensities.

The development of a method for noninvasive measurement of temperature at depth has practical applications in a variety of fields including biomedical monitoring, catalytic research, and process monitoring. Apart from monitoring temperature in depth in samples with thermal gradients the method also enables the measurements of nonequilibrated systems where chemically distinct entities are at different temperature from their surroundings (e.g., a chemical reaction in progress with direct monitoring of reagents or catalysts).

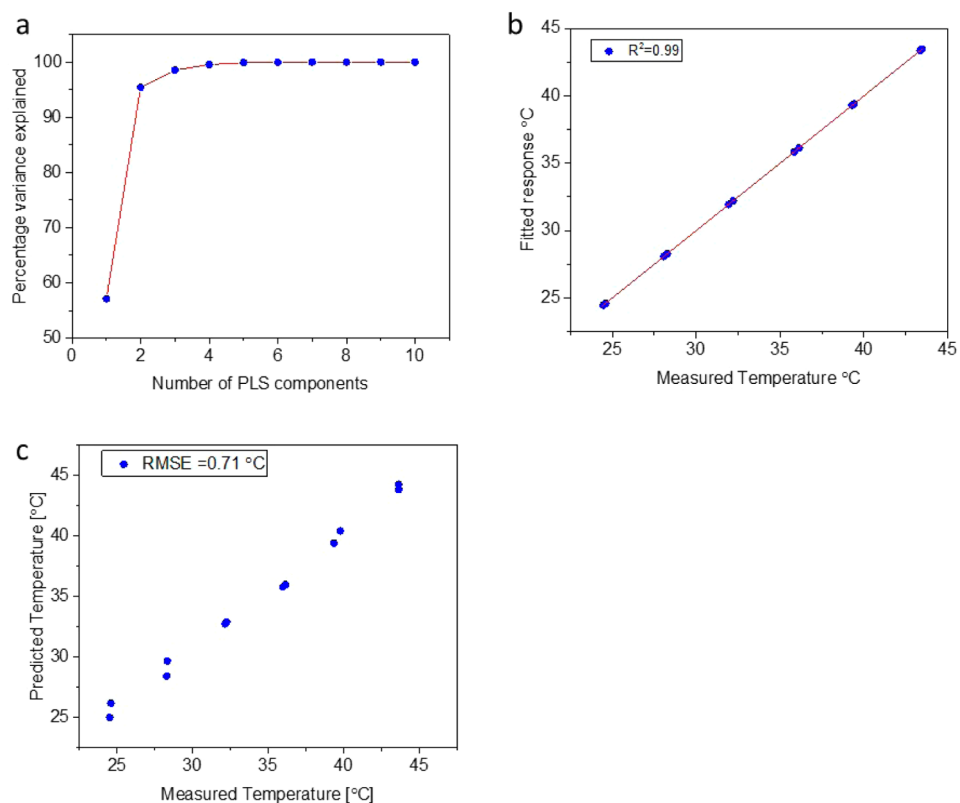


**Figure 5.** PLS models of heating (24–44 °C). (a) The percentage of variance explained for the sets of replica data, as a function of the number of components used in the PLS model of PTFE being heated behind a layer of POM. (b) The fit response vs observed response for the PLS model (calibration data set). (c) Predicted temperatures vs the measured temperature for PTFE behind POM for the final test set of data (prediction data set).

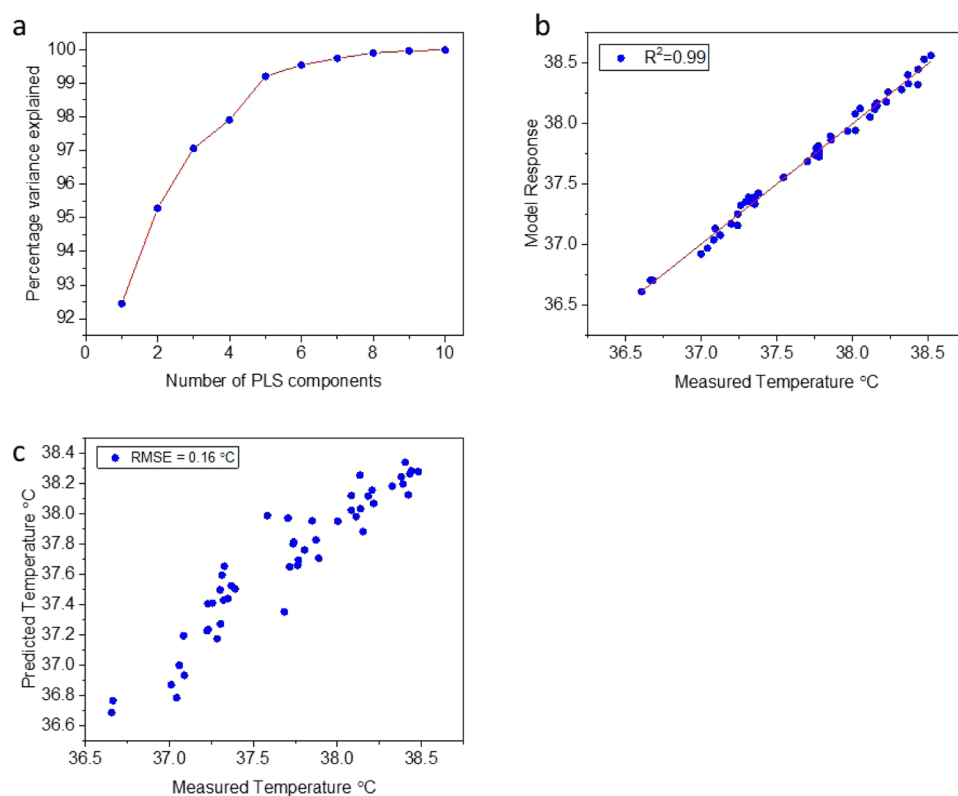


**Figure 6.** PLS models of heating (36–39 °C). (a) The percentage of variance explained for all four sets of replica data, as a function of the number of components used in the PLS model of PTFE being heated behind a layer of POM. (b) The fit response vs observed response for the PLS model. (c) Predicted temperatures vs the measured temperature for PTFE behind POM for the final test set of data.

## AUTHOR INFORMATION

### Corresponding Authors

\*E-mail: pavel.matousek@stfc.ac.uk.

\*E-mail: N.stone@exeter.ac.uk.

### Notes

The authors declare no competing financial interest.

## ACKNOWLEDGMENTS

This project was partly supported by a grant from the Engineering and Physical Sciences Research Council, U.K. [EP/K020374/1].

## REFERENCES

- (1) Bagavathiappan, S.; Lahiri, B. B.; Saravanan, T.; Philip, J.; Jayakumar, T. *Infrared Phys. Technol.* **2013**, *60*, 35–55.
- (2) Rogalski, A.; Antoszewski, J.; Faraone, L. *J. Appl. Phys.* **2009**, *105*, 091101.
- (3) Levick, A.; Land, D.; Hand, J. *Meas. Sci. Technol.* **2011**, *22*, 065801.
- (4) Hynynen, K.; McDannold, N.; Mulkern, R. V.; Jolesz, F. A. *Magn. Reson. Med.* **2000**, *43*, 901–904.
- (5) Baokun, H.; Yanjie, T.; Zuowei, L.; Shuquin, G.; Zhaokai, L. *Instrum. Exp. Tech.* **2007**, *50*, 282–285.
- (6) Smith, E.; Dent, G. *Modern Raman Spectroscopy—A Practical Approach*; John Wiley & Sons Ltd.: Chichester, U.K., 2005; Chapter 6.
- (7) Matousek, P.; Clark, I. P.; Draper, E. R. C.; Morris, M. D.; Goodship, A. E.; Everall, N.; Towrie, M.; Finney, W. F.; Parker, A. W. *Appl. Spectrosc.* **2005**, *59* (4), 393–400.
- (8) Matousek, P.; Morris, M. D.; Everall, N.; Clark, I. P.; Towrie, M.; Draper, E.; Goodship, A.; Parker, A. W. *Appl. Spectrosc.* **2005**, *59* (12), 1485–1492.
- (9) Buckley, K.; Matousek, P. *Analyst* **2011**, *136*, 3039–3050.
- (10) Matousek, P.; Stone, N. *J. Biophotonics* **2013**, *6*, 7–19.
- (11) Matousek, P. *Appl. Spectrosc.* **2006**, *60* (11), 1341–7.